Journal of Cell Science (2015) 128, 232–238 doi:10.1242/jcs.164152

morphology was normalised in LRRK2-PD fibroblasts transfected with a siRNA against TPC2. Quantitative PCR confirmed selective knockdown of TPC2 transcripts in siRNA-treated cells (Fig. 2F). Intriguingly, we noted little effect of TPC1 silencing on lysosomal morphology in LRRK2-PD fibroblasts (Fig. 2D,E) despite demonstrable knockdown at both the transcript (Fig. 2F) and protein (supplementary material Fig. S2B) level.

Exaggerated perinuclear clustering of lysosomes in LRRK2-PD cells (Fig. 1) is consistent with the actions of both TPC2 (Lin-Moshier et al., 2014) and Rab7 (Bucci et al., 2000; Hutagalung and Novick, 2011). We therefore tested the effects of inhibiting Rab7 GTPase activity (Agola et al., 2012) on lysosomal morphology and distribution in LRRK2-PD fibroblasts. Importantly, lysosomal defects in LRRK2-PD cells were corrected upon Rab7 inhibition (Fig. 2G K; supplementary material Fig. S3). This reversal was concentration dependent (Fig. 2L). Levels of endogenous VPS35, a component of the retromer complex (MacLeod et al., 2013), were unchanged in our LRRK2-PD fibroblasts compared to controls (supplementary material Fig. S2A). Taken together, data presented here reveal a specific role for TPC2 and a newly identified interactor (Rab 7) in regulating lysosomal morphology in LRRK2-PD cells.

### Lysosomal morphology defects are dependent on NAADP and PtdIns(3,5)$P_2$

Much evidence has accumulated identifying TPCs as the long-sought endolysosomal targets for NAADP (Brailoiu et al., 2009; Calcraft et al., 2009; Hooper and Patel, 2012; Zong et al., 2009). Notably, NAADP-induced $Ca^{2+}$ release is inhibited when TPCs are silenced or genetically deleted (Brailoiu et al., 2009; Calcraft et al., 2009; Davis et al., 2012; Dionisio et al., 2011; Grimm et al.,

Fig. 2. TPC2 but not TPC1 mediates lysosomal morphology disturbances. (A–D) LAMP1 staining in fibroblasts from a healthy control (CTRL) (A) and a Parkinson disease patient (PD) (B–D) treated with either a control siRNA (Scr. siRNA) (A,B) or siRNA to TPC2 (C) or TPC1 (D). Scale bars: 5 μm. (E) Pooled data quantifying LAMP1 intensity for the cells shown in A–D (mean6 s.e.m., *n*5 381–532 cells from six independent knockdowns from two patient and paired control lines). (F) Quantitative PCR analysis of TPC2 (left) and TPC1 (right) levels in cells treated with the indicated TPC siRNA. Data are from two patients and are normalised to TPC levels in cells treated with scrambled control siRNA. (G–I) Lysosomal morphology in control fibroblasts (G) or LRRK2-PD fibroblasts treated without (H) or with (I) the Rab7 GTPase inhibitor CID 1067700 (1 μM, 3 days). (J,K) Pooled data quantifying LAMP1 intensity (J) or the proportion of cells displaying perinuclear lysosome clustering (K) for the cells shown in G–I (mean6 s.e.m., *n*5 237–281 cells from five independent platings of three patient and paired control lines). ***$P$, 0.001. (L) Concentration–effect relationship (mean6 s.e.m., *n*5 130–281 cells from five independent platings of three patient lines) for the Rab7 GTPase inhibitor on lysosome clustering in LRRK2-PD fibroblasts.

incubated with 100 nM LysotrackerH red (Invitrogen) for 20 min. Cells were washed again three times in HBS, and mounted in an imaging chamber (Biosciences Tools) prior to confocal microscopy.

### Immunocytochemistry

Fibroblasts were fixed for 10 min with 4% (w/v) paraformaldehyde, washed three times in phosphate-buffered saline (PBS) and then permeabilised for 10 min with 40 mM β-escin. Cells were washed again (three times in PBS), and blocked for 1 h with PBS supplemented with 1% (w/v) BSA and 10% (v/v) FBS. Fibroblasts were sequentially incubated for 1 h at 37 C with a primary anti-LAMP1 antibody (mouse, Developmental Studies Hybridoma Bank H4A3 clone supernatant; 1:10 dilution) and a secondary antibody conjugated to Alexa Fluor 647 (mouse, Invitrogen, 1:100 dilution) in blocking solution. Nuclei were labelled with 1 mg/ml DAPI (5 min). Cells were washed three times in PBS containing 0.1% (v/v) TweenH 20 in between incubations and mounted onto microscope slides with DABCO.

### Microscopy

Confocal images were captured using an LSM510 confocal scanner (Zeiss) attached to a Zeiss Axiovert 200M inverted microscope fitted with a 636 Plan Apochromat water-immersion objective. DAPI, LysotrackerH Red and Alexa Fluor 647 were excited at 364 nm, 543 nm and 633 nm, and emitted fluorescence captured using 385 nm long pass, 585 615 nm band-pass or 655 719 nm band-pass filters, respectively. Images for control and LRRK2-PD cells together with the various treatments were captured under identical acquisition settings in order to allow comparison of fluorescent intensity. Electron microscopy was performed as described previously (Tomas et al., 2004) using a JEOL 1010 transmission electron microscope.

### Quantitative PCR

Total RNA was isolated using TRIzolH (Invitrogen) according to the manufacturer s procedures. cDNA was synthesised using SuperScriptH III reverse transcriptase (Invitrogen). Samples were denatured for 2 min at 94 C followed by 40 cycles of denaturation (15 s, 94 C), annealing (30 s, 60 C) and extension (30 s, 72 C) using SYBRH Green PCR mix (Invitrogen) and oligonucleotide primers designed for human TPC1 and TPC2 as previously described (Brailoiu et al., 2009). Expression levels were normalised to the expression of GAPDH following parallel amplification.

### Western blotting

Fibroblasts were harvested by scraping and lysed in Ripa buffer containing 150 mM NaCl, 50 mM Tris-HCl (pH 7.4), 0.5% sodium deoxycholic acid, 0.1% sodium dodecyl sulphate and 1% Triton X-100 in the presence of EDTA-free protease inhibitor (Roche) and Halt™ phosphatase inhibitor cocktail (Thermo Scientific) for 30 min on ice. Samples were centrifuged at 15,000 g at 4 C for 15 min and the resulting supernatants stored at 2 20 C until required. Samples (10 30 mg) were reduced with dithiothreitol (100 mM), separated on NuPAGEH 4 12% Bis-Tris gels (Invitrogen) and transferred onto PVDF filters (Biorad) according to standard procedures. The filters were then blocked with 5% (w/v) dried skimmed milk in Tris-buffered saline (25 mM Tris-HCl, 137 mM NaCl and 2.7 mM KCl, pH 7.4) containing 0.1% (v/v) TweenH 20 (TBS-T) for either 1 h at room temperature or overnight at 4 C. Blots were sequentially incubated with primary and secondary antibodies in TBS-T supplemented with 2.5% (w/v) dried skimmed milk. After each step, the filters were washed with TBS-T (36 30 min). The resulting blots were developed using the ECL™ Prime Western Blot Detection System (GE Healthcare) according to the manufacturer s instructions. The primary antibodies used were anti-LAMP1 (mouse, Santa Cruz Biotechnology; 1:500, overnight 4 C), anti-TPC1 (rabbit, Abcam, 1:200, 1 h room temperature), anti-VPS35 (rabbit, Abcam, 1:1000, overnight 4 C) and anti-actin (goat, Invitrogen, 1:500, 1 h room temperature) antibodies. The secondary antibodies used were anti-mouse-IgG (Santa Cruz Biotechnology), anti-rabbit-IgG (Bio-Rad) or anti-goat-IgG (Santa Cruz Biotechnology) conjugated to horseradish peroxidase (1:2000, 1 h room temperature).

### $Ca^{2+}$ imaging and microinjection

Cytosolic $Ca^{2+}$ concentration measurements using Fura-2 and microinjection were performed as described previously (Deliu et al., 2012).

### Data analysis

Images were analysed using ImageJ software. For LysotrackerH red and LAMP1 intensity measurements, background was subtracted from the images and mean grey intensity per cell measured within user defined regions-of-interest (comprising the whole lysosome population). Statistical analyses were performed using IBM SPSS statistics 22 software. Independent Student s *t*-tests or one-way ANOVA followed by Games Howell post hoc tests were applied to calculate statistical significance. Values are presented as mean6 s.e.m. For ANOVA analysis, threshold of significance was maintained at $P$, 0.016 to correct for multiple testing error.

### Acknowledgements

We thank A. Ganesan (University of East Anglia), Raj Gossain (University of Southampton) and Sean M. Davidson (Hatter Institute, UCL) for providing the NAADP antagonists, Jan-Willem Taanman and Tania Papkovskaia (Institute of Neurology, UCL) for help with fibroblasts and Mary Rahman (UCL) for technical assistance.

### Competing interests

The authors declare no competing interests.

### Author contributions

L.N.H. and B.S.K. performed the cell culture, siRNA treatments, immunocytochemistry, confocal microscopy and western blotting. L.N.H., G.C.B. and E.B. performed the $Ca^{2+}$ imaging and microinjection. Y.L. performed the quantitative PCR. E.R.E. performed the electron microscopy. A.H.S. provided the fibroblasts. C.E.F., A.H.S., J.S.M. and S.P. conceived the study. S.P. wrote the paper with input from all authors.

### Funding

This work was supported by grants from Parkinson's UK (to S.P. and A.H.S.); the National Institutes of Health [grant number GM088790 to J.S.M.], a Wellcome Trust/MRC Joint Call in Neurodegeneration award [grant number WT089698 to A.H.S.]; a Medical Research Council CoEN award (to A.H.S.). A.H.S. is a National Institute for Health Research Senior Investigator. B.S.K. was a recipient of a UCL IMPACT studentship. Deposited in PMC for immediate release.

### Supplementary material

Supplementary material available online at
http://jcs.biologists.org/lookup/suppl/doi:10.1242/jcs.164152/-/DC1

### References

Agola, J. O., Hong, L., Surviladze, Z., Ursu, O., Waller, A., Strouse, J. J., Simpson, D. S., Schroeder, C. E., Oprea, T. I., Golden, J. E. et al. (2012). A competitive nucleotide binding inhibitor: in vitro characterization of Rab7 GTPase inhibition. *ACS Chem. Biol.* 7, 1095-1108.

Alegre-Abarrategui, J., Christian, H., Lufino, M. M., Mutihac, R., Venda, L. L., Ansorge, O. and Wade-Martins, R. (2009). LRRK2 regulates autophagic activity and localizes to specific membrane microdomains in a novel human genomic reporter cellular model. *Hum. Mol. Genet.* 18, 4022-4034.

Biskup, S., Moore, D. J., Celsi, F., Higashi, S., West, A. B., Andrabi, S. A., Kurkinen, K., Yu, S. W., Savitt, J. M., Waldvogel, H. J. et al. (2006). Localization of LRRK2 to membranous and vesicular structures in mammalian brain. *Ann. Neurol.* 60, 557-569.

Brailoiu, E., Churamani, D., Cai, X., Schrlau, M. G., Brailoiu, G. C., Gao, X., Hooper, R., Boulware, M. J., Dun, N. J., Marchant, J. S. et al. (2009). Essential requirement for two-pore channel 1 in NAADP-mediated calcium signaling. *J. Cell Biol.* 186, 201-209.

Brailoiu, E., Rahman, T., Churamani, D., Prole, D. L., Brailoiu, G. C., Hooper, R., Taylor, C. W. and Patel, S. (2010). An NAADP-gated two-pore channel targeted to the plasma membrane uncouples triggering from amplifying $Ca^{2+}$ signals. *J. Biol. Chem.* 285, 38511-38516.

Bucci, C., Thomsen, P., Nicoziani, P., McCarthy, J. and van Deurs, B. (2000). Rab7: a key to lysosome biogenesis. *Mol. Biol. Cell* 11, 467-480.

Calcraft, P. J., Ruas, M., Pan, Z., Cheng, X., Arredouani, A., Hao, X., Tang, J., Rietdorf, K., Teboul, L., Chuang, K. T. et al. (2009). NAADP mobilizes calcium from acidic organelles through two-pore channels. *Nature* 459, 596-600.

Cookson, M. R. (2010). The role of leucine-rich repeat kinase 2 (LRRK2) in Parkinson's disease. *Nat. Rev. Neurosci.* 11, 791-797.

Davis, L. C., Morgan, A. J., Chen, J. L., Snead, C. M., Bloor-Young, D., Shenderov, E., Stanton-Humphreys, M. N., Conway, S. J., Churchill, G. C.,

Parrington, J. et al. (2012). NAADP activates two-pore channels on T cell cytolytic granules to stimulate exocytosis and killing. *Curr. Biol.* 22, 2331-2337.
Deliu, E., Brailoiu, G. C., Mallilankaraman, K., Wang, H., Madesh, M., Undieh, A. S., Koch, W. J. and Brailoiu, E. (2012). Intracellular endothelin type B receptor-driven Ca2+ signal elicits nitric oxide production in endothelial cells. *J. Biol. Chem.* 287, 41023-41031.
Deng, X., Dzamko, N., Prescott, A., Davies, P., Liu, Q., Yang, Q., Lee, J. D., Patricelli, M. P., Nomanbhoy, T. K., Alessi, D. R. et al. (2011). Characterization of a selective inhibitor of the Parkinson's disease kinase LRRK2. *Nat. Chem. Biol.* 7, 203-205.
Dionisio, N., Albarra·n, L., Lo pez, J. J., Berna-Erro, A., Salido, G. M., Bobe, R. and Rosado, J. A. (2011). Acidic NAADP-releasable Ca(2+) compartments in the megakaryoblastic cell line MEG01. *Biochim. Biophys. Acta* 1813, 1483-1494.
Dodson, M. W., Zhang, T., Jiang, C., Chen, S. and Guo, M. (2012). Roles of the Drosophila LRRK2 homolog in Rab7-dependent lysosomal positioning. *Hum. Mol. Genet.* 21, 1350-1363.
Gɔmez-Suaga, P., Luzo n-Toro, B., Churamani, D., Zhang, L., Bloor-Young, D., Patel, S., Woodman, P. G., Churchill, G. C. and Hilfiker, S. (2012). Leucine-rich repeat kinase 2 regulates autophagy through a calcium-dependent pathway involving NAADP. *Hum. Mol. Genet.* 21, 511-525.
Grimm, C., Holdt, L. M., Chen, C. C., Hassan, S., Mu¤ller, C., Jɑrs, S., Cuny, H., Kissing, S., Schro¤der, B., Butz, E. et al. (2014). High susceptibility to fatty liver disease in two-pore channel 2-deficient mice. *Nat. Commun.* 5, 4699.
Hardy, J. (2010). Genetic analysis of pathways to Parkinson disease. *Neuron* 68, 201-206.
Healy, D. G., Falchi, M., O Sullivan, S. S., Bonifati, V., Durr, A., Bressman, S., Brice, A., Aasly, J., Zabetian, C. P., Goldwurm, S. et al.; International LRRK2 Consortium (2008). Phenotype, genotype, and worldwide genetic penetrance of LRRK2-associated Parkinson's disease: a case-control study. *Lancet Neurol.* 7, 583-590.
Hooper, R. and Patel, S. (2012). NAADP on target. *Adv. Exp. Med. Biol.* 740, 325-347.
Hutagalung, A. H. and Novick, P. J. (2011). Role of Rab GTPases in membrane traffic and cell physiology. *Physiol. Rev.* 91, 119-149.
Jefferies, H. B., Cooke, F. T., Jat, P., Boucheron, C., Koizumi, T., Hayakawa, M., Kaizawa, H., Ohishi, T., Workman, P., Waterfield, M. D. et al. (2008). A selective PIKfyve inhibitor blocks PtdIns(3,5)P(2) production and disrupts endomembrane transport and retroviral budding. *EMBO Rep.* 9, 164-170.
Jha, A., Ahuja, M., Patel, S., Brailoiu, E. and Muallem, S. (2014). Convergent regulation of the lysosomal two-pore channel-2 by $Mg^{2+}$, NAADP, $PI(3,5)P_2$ and multiple protein kinases. *EMBO J.* 33, 501-511.
Korolchuk, V. I., Saiki, S., Lichtenberg, M., Siddiqi, F. H., Roberts, E. A., Imarisio, S., Jahreiss, L., Sarkar, S., Futter, M., Menzies, F. M. et al. (2011). Lysosomal positioning coordinates cellular nutrient responses. *Nat. Cell Biol.* 13, 453-460.
Lin-Moshier, Y., Keebler, M. V., Hooper, R., Boulware, M. J., Liu, X., Churamani, D., Abood, M. E., Walseth, T. F., Brailoiu, E., Patel, S. et al. (2014). The Two-pore channel (TPC) interactome unmasks isoform-specific roles for TPCs in endolysosomal morphology and cell pigmentation. *Proc. Natl. Acad. Sci. USA* 111, 13087-13092.
Lu, Y., Hao, B. X., Graeff, R., Wong, C. W., Wu, W. T. and Yue, J. (2013). Two pore channel 2 (TPC2) inhibits autophagosomal-lysosomal fusion by alkalinizing lysosomal pH. *J. Biol. Chem.* 288, 24247-24263.
Luzio, J. P., Pryor, P. R. and Bright, N. A. (2007). Lysosomes: fusion and function. *Nat. Rev. Mol. Cell Biol.* 8, 622-632.
MacLeod, D. A., Rhinn, H., Kuwahara, T., Zolin, A., Di Paolo, G., McCabe, B. D., Marder, K. S., Honig, L. S., Clark, L. N., Small, S. A. et al. (2013). RAB7L1 interacts with LRRK2 to modify intraneuronal protein sorting and Parkinson's disease risk. *Neuron* 77, 425-439.
Morgan, A. J., Davis, L. C., Wagner, S. K., Lewis, A. M., Parrington, J., Churchill, G. C. and Galione, A. (2013). Bidirectional $Ca^{2+}$ signaling occurs between the endoplasmic reticulum and acidic organelles. *J. Cell Biol.* 200, 789-805.
Naylor, E., Arredouani, A., Vasudevan, S. R., Lewis, A. M., Parkesh, R., Mizote, A., Rosen, D., Thomas, J. M., Izumi, M., Ganesan, A. et al. (2009). Identification of a chemical probe for NAADP by virtual screening. *Nat. Chem. Biol.* 5, 220-226.
Nixon, R. A., Yang, D. S. and Lee, J. H. (2008). Neurodegenerative lysosomal disorders: a continuum from development to late age. *Autophagy* 4, 590-599.
Paisan-Ru·z, C., Jain, S., Evans, E. W., Gilks, W. P., Simo·n, J., van der Brug, M., Lɵpez de Munain, A., Aparicio, S., Gil, A. M., Khan, N. et al. (2004). Cloning of the gene containing mutations that cause PARK8-linked Parkinson's disease. *Neuron* 44, 595-600.
Papkovskaia, T. D., Chau, K. Y., Inesta-Vaquera, F., Papkovsky, D. B., Healy, D. G., Nishio, K., Staddon, J., Duchen, M. R., Hardy, J., Schapira, A. H. et al. (2012). G2019S leucine-rich repeat kinase 2 causes uncoupling protein-mediated mitochondrial depolarization. *Hum. Mol. Genet.* 21, 4201-4213.
Pryor, P. R., Mullock, B. M., Bright, N. A., Gray, S. R. and Luzio, J. P. (2000). The role of intraorganellar $Ca^{(2+)}$ in late endosome-lysosome heterotypic fusion and in the reformation of lysosomes from hybrid organelles. *J. Cell Biol.* 149, 1053-1062.
Reith, A. D., Bamborough, P., Jandu, K., Andreotti, D., Mensah, L., Dossang, P., Choi, H. G., Deng, X., Zhang, J., Alessi, D. R. et al. (2012). GSK2578215A; a potent and highly selective 2-arylmethyloxy-5-substitutent-N-arylbenzamide LRRK2 kinase inhibitor. *Bioorg. Med. Chem. Lett.* 22, 5625-5629.
Ruas, M., Rietdorf, K., Arredouani, A., Davis, L. C., Lloyd-Evans, E., Koegel, H., Funnell, T. M., Morgan, A. J., Ward, J. A., Watanabe, K. et al. (2010). Purified TPC isoforms form NAADP receptors with distinct roles for $Ca^{(2+)}$ signaling and endolysosomal trafficking. *Curr. Biol.* 20, 703-709.
Ruas, M., Chuang, K. T., Davis, L. C., Al-Douri, A., Tynan, P. W., Tunn, R., Teboul, L., Galione, A. and Parrington, J. (2014). TPC1 has two variant isoforms and their removal has different effects on endo-lysosomal functions compared to loss of TPC2. *Mol. Cell Biol*. [Epub ahead of print] doi: 10.1128/MCB.00113-14.
Sardiello, M., Palmieri, M., di Ronza, A., Medina, D. L., Valenza, M., Gennarino, V. A., Di Malta, C., Donaudy, F., Embrione, V., Polishchuk, R. S. et al. (2009). A gene network regulating lysosomal biogenesis and function. *Science* 325, 473-477.
Schapira, A. H. and Jenner, P. (2011). Etiology and pathogenesis of Parkinson's disease. *Mov. Disord.* 26, 1049-1055.
Shin, N., Jeong, H., Kwon, J., Heo, H. Y., Kwon, J. J., Yun, H. J., Kim, C. H., Han, B. S., Tong, Y., Shen, J. et al. (2008). LRRK2 regulates synaptic vesicle endocytosis. *Exp. Cell Res.* 314, 2055-2065.
te Vruchte, D., Speak, A. O., Wallom, K. L., Al Eisa, N., Smith, D. A., Hendriksz, C. J., Simmons, L., Lachmann, R. H., Cousins, A., Hartung, R. et al. (2014). Relative acidic compartment volume as a lysosomal storage disorder-associated biomarker. *J. Clin. Invest.* 124, 1320-1328.
Tomas, A., Futter, C. and Moss, S. E. (2004). Annexin 11 is required for midbody formation and completion of the terminal phase of cytokinesis. *J. Cell Biol.* 165, 813-822.
Wang, X., Zhang, X., Dong, X. P., Samie, M., Li, X., Cheng, X., Goschka, A., Shen, D., Zhou, Y., Harlow, J. et al. (2012). TPC proteins are phosphoinositide-activated sodium-selective ion channels in endosomes and lysosomes. *Cell* 151, 372-383.
West, A. B., Moore, D. J., Biskup, S., Bugayenko, A., Smith, W. W., Ross, C. A., Dawson, V. L. and Dawson, T. M. (2005). Parkinson's disease-associated mutations in leucine-rich repeat kinase 2 augment kinase activity. *Proc. Natl. Acad. Sci. USA* 102, 16842-16847.
Zimprich, A., Biskup, S., Leitner, P., Lichtner, P., Farrer, M., Lincoln, S., Kachergus, J., Hulihan, M., Uitti, R. J., Calne, D. B. et al. (2004). Mutations in LRRK2 cause autosomal-dominant parkinsonism with pleomorphic pathology. *Neuron* 44, 601-607.
Zong, X., Schieder, M., Cuny, H., Fenske, S., Gruner, C., Ro¤tzer, K., Griesbeck, O., Harz, H., Biel, M. and Wahl-Schott, C. (2009). The two-pore channel TPCN2 mediates NAADP-dependent $Ca^{(2+)}$-release from lysosomal stores. *Pflugers Arch.* 458, 891-899.

**Fig. S1. Pathogenic LRRK2 disrupts lysosomal morphology in multiple patients. A-C**, LAMP1 staining in fibroblasts derived from healthy controls (left) and age-matched PD patients harbouring the LRRK2 G2019S mutation (right). Scale bars, 5 µm. **D-E**, Summary data for each control/patient pair quantifying LAMP1 intensity (**D**) or the proportion of cells displaying perinuclear lysosome clustering (**E**). Data are from 93-555 healthy control and 102-582 LRRK2-PD cells. Right panels show aggregate data for all four experimental pairs used in this study incorporating data from Fig. 1. $**p<0.01$; $***p<0.001$

**Fig. S2. Quantification of endogenous LAMP1, VPS35 and TPC levels in human fibroblasts. A**, Western blot analysis using antibodies to LAMP1 (left) or VPS35 (right) and fibroblast homogenates prepared from a healthy control or LRRK2-PD patient (10 µg, LAMP1; 30 µg VPS35). Blots were stripped and re-probed using an antibody to actin (bottom panels). Migration of molecular mass markers (in kDa) is shown on the left. Results of densitometric analysis quantifying the fold-change in protein levels in PD patients versus healthy control (3 pairs, 2-5 determinations per individual) are listed at the bottom. **B**, Western blot analysis using an antibody to TPC1 and fibroblast homogenates prepared from a LRRK2-PD patient (17 µg) that were treated with a scrambled siRNA or siRNA to TPC1 or TPC2. Results of densitometeric analysis quantifying the fold-change in TPC1 levels (bracketed area) in TPC siRNA-treated cells relative to scrambled siRNA (3 independent knock downs from 2 patients).

**Fig. S3. Lysosomal defects are reversed by acute inhibition of LRRK2 kinase, Rab7 and NAADP. A-H**. LAMP1 staining in fibroblasts from a healthy control (**A**) and a PD patient (**B-H**) treated for the indicated time with LRRK2-In1 (100 nM, **C-D**), the Rab7 GTPase

inhibitor, CID 1067700 (1 µM, **E**), Ned-19 (100 µM, **F-G**) and Ned-K (100 µM**, H).** Scale bars, 5 µm. **I,** Pooled data (n=50-78 cells). *** $p<0.001$.

**Fig. S4. Pathogenic LRRK2 disrupts lysosomal ultrastructure.** Electron micrograph of a LRRK2-PD fibroblast. Example of an hour-glass structure (*). Scale bar, 500 nm.

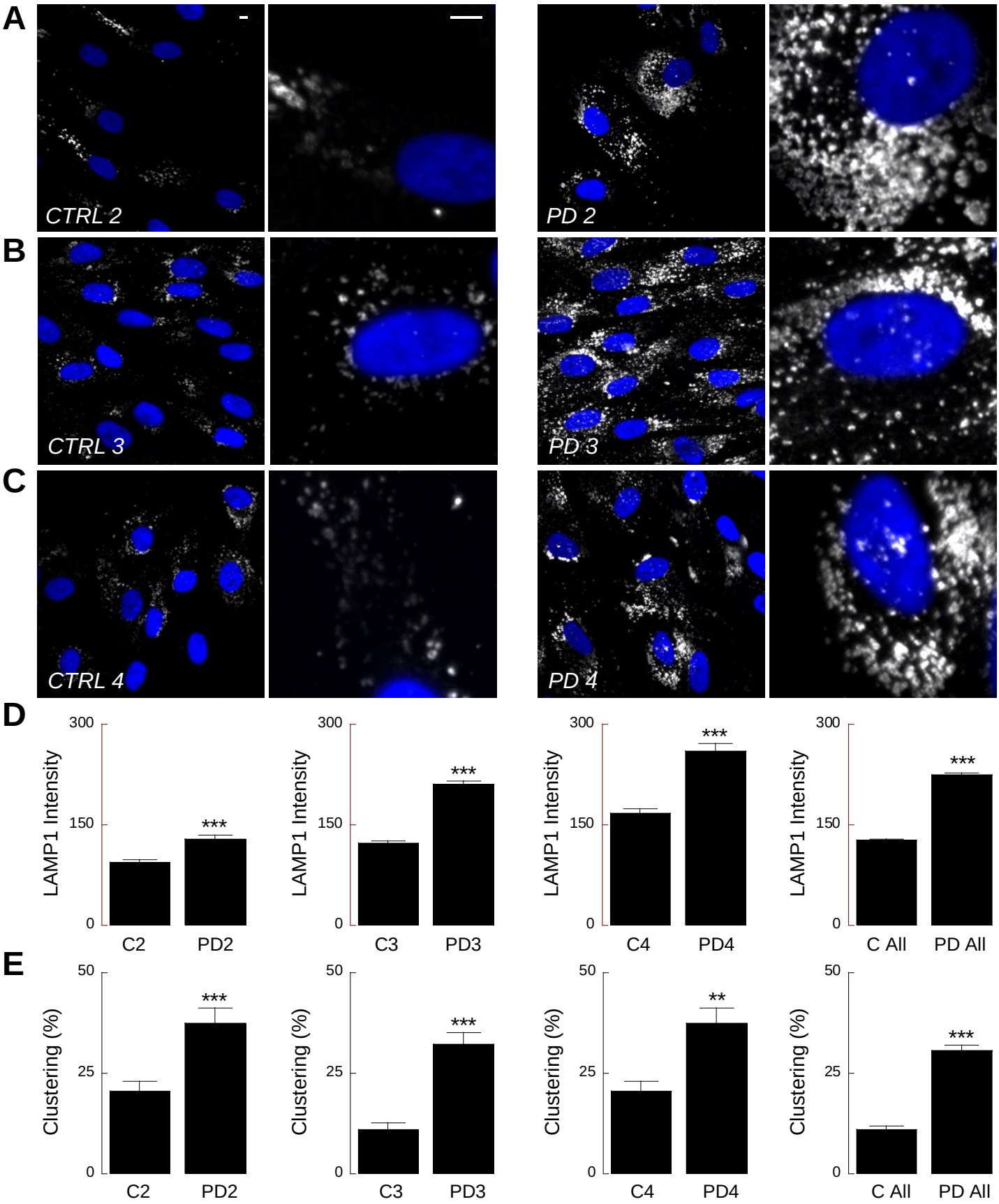
A
CTRL 2
PD 2
B
CTRL 3
PD 3
C
CTRL 4
PD 4
D
LAMP1 Intensity
300
150
0
***
C2
PD2
C3
PD3
C4
PD4
C All
PD All
E
Clustering (%)
50
25
0
**

Figure S1

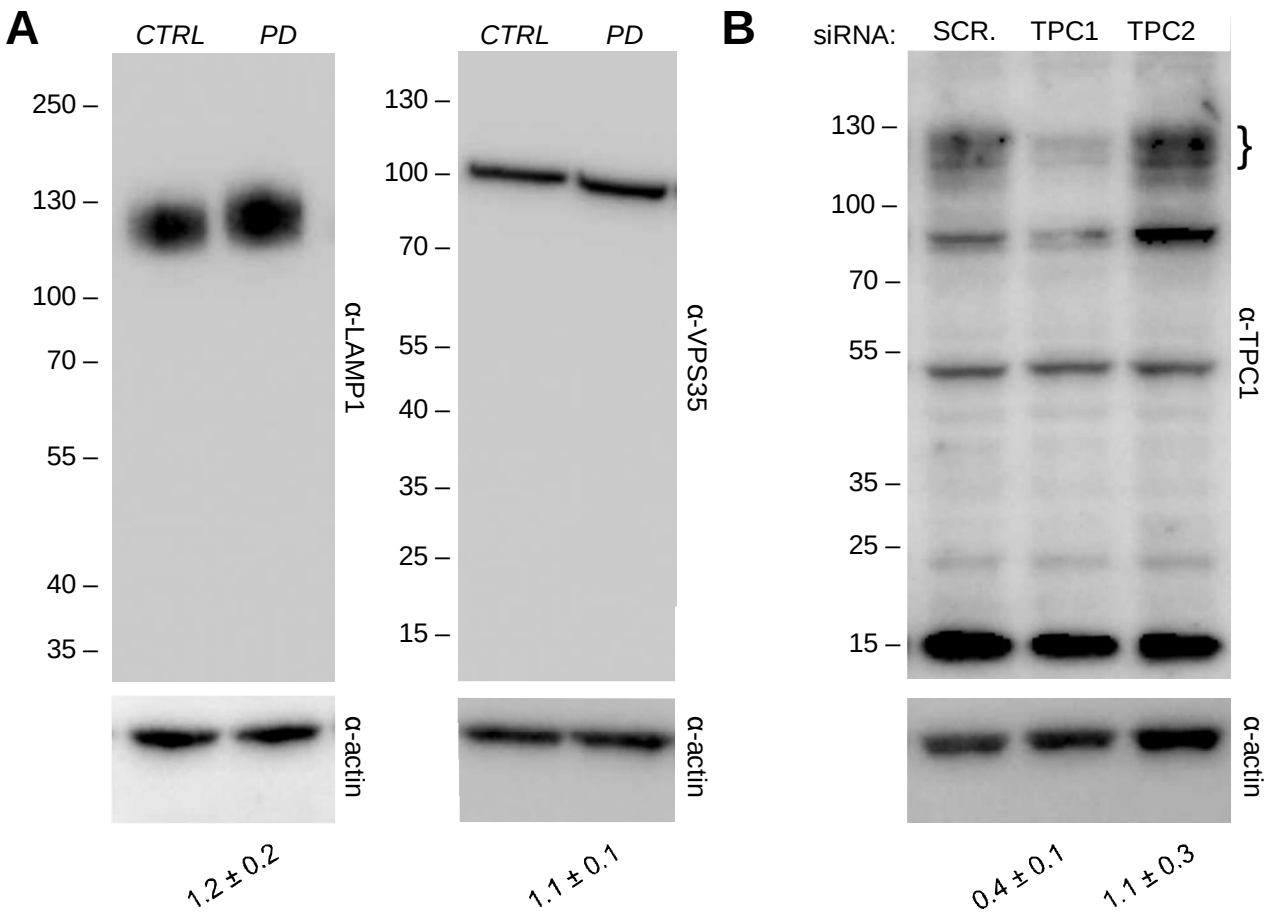
A
CTRL
PD
250 –
130 –
100 –
70 –
55 –
40 –
35 –
α-LAMP1
α-actin
1.2 ± 0.2
CTRL
PD
130 –
100 –
70 –
55 –
40 –
35 –
25 –
15 –
α-VPS35
α-actin
1.1 ± 0.1
B
siRNA:
SCR.
TPC1
TPC2
130 –
100 –
70 –
55 –
35 –
25 –
15 –
α-TPC1
α-actin
0.4 ± 0.1
1.1 ± 0.3

Figure S2

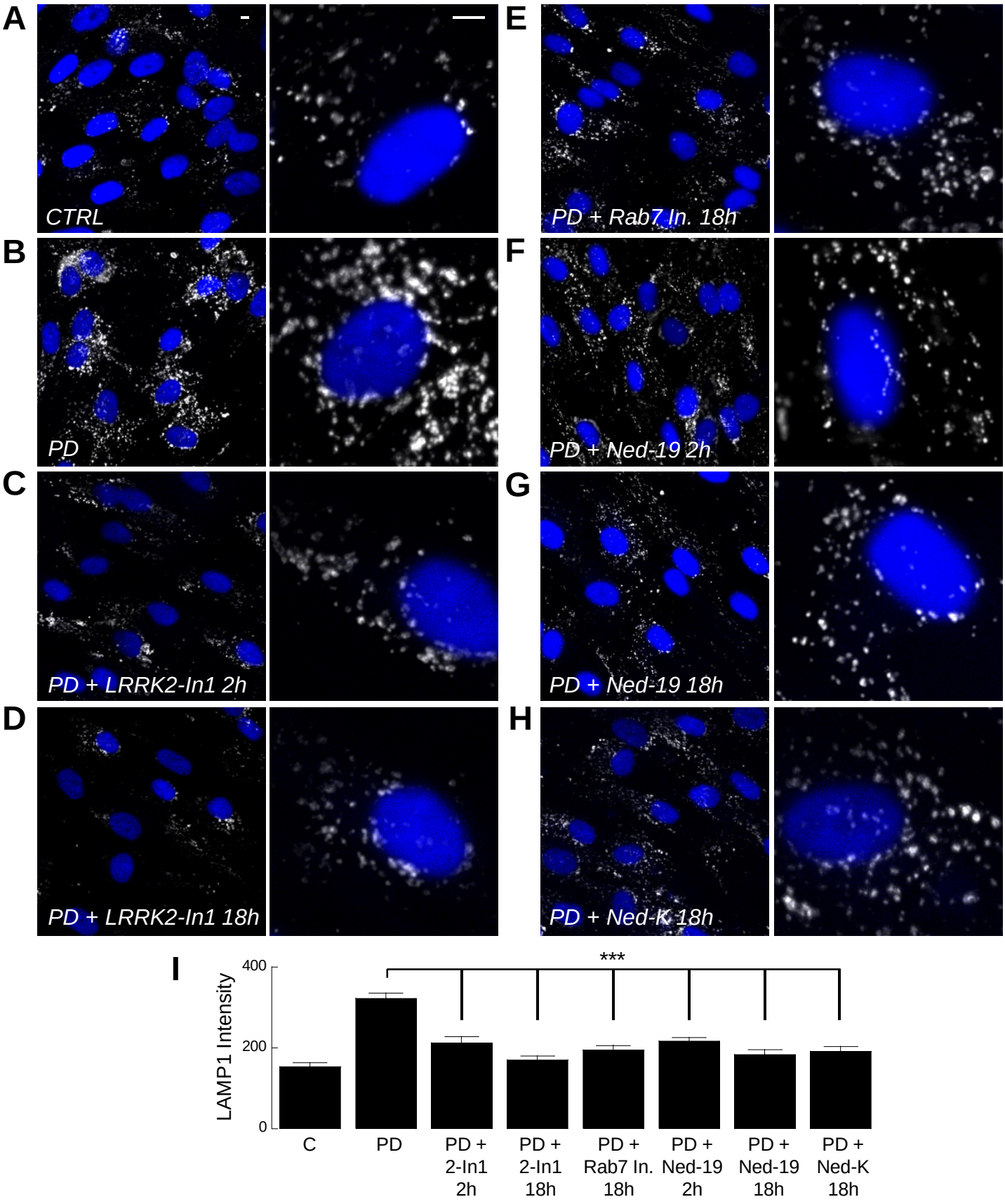
A
CTRL
B
PD
C
PD + LRRK2-In1 2h
D
PD + LRRK2-In1 18h
E
PD + Rab7 In. 18h
F
PD + Ned-19 2h
G
PD + Ned-19 18h
H
PD + Ned-K 18h
I
LAMP1 Intensity
400
200
0
***
C
PD
PD + 2-In1 2h
PD + 2-In1 18h
PD + Rab7 In. 18h
PD + Ned-19 2h
PD + Ned-19 18h
PD + Ned-K 18h

Figure S3

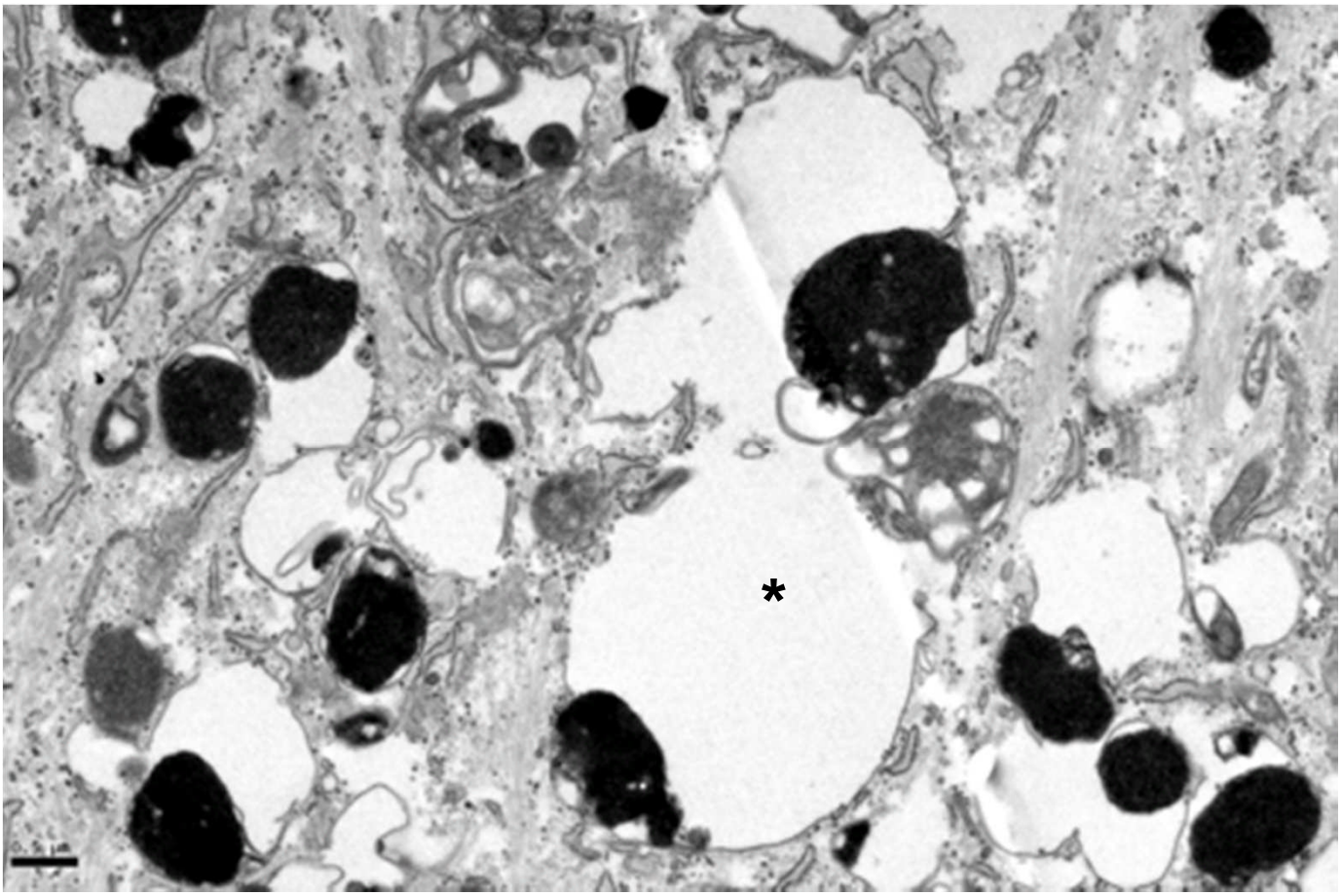


Figure S4